A Heterogeneous Prognosis Prediction Framework with Global Brain Connectivity and Local Image Features

Jingfeng Lin[1], Junjun Pan[1,2], Jinda Wang[3], and Zhenyu Tang[1,2(✉)]

[1] Beihang University, Beijing 100191, China
[2] State Key Laboratory of Virtual Reality Technology and System, Beihang University, Beijing 100191, China
[3] Sixth Medical Center, Chinese PLA General Hospital, Beijing 100853, China
tangzhenyu@buaa.edu.cn

Abstract. Diffuse glioma is the most prevalent malignant brain tumor, and accurate prognosis prediction is essential in personalized treatment to improve outcomes. Although numerous deep learning based methods have been proposed for prognosis prediction, most of them rely solely on local image features of tumor regions. They neglect the fact that the brain is an integrated and highly interconnected system, and tumors can disrupt the global brain connectivity, which is closely associated with prognosis. To address this limitation, we present a novel heterogeneous framework that integrates global brain connectivity and local image features for prognosis prediction. Specifically, our framework consists of a DTI based graph neural network (GNN) and a structural MR based local feature network (LFN), which are coupled through an iterative pipeline. In each iteration, the GNN models the global connectivity among brain regions (nodes) with consideration of brain compensation caused by tumor disruptions, while the LFN leverages the resulting global brain connectivity to extract effective local image features from each brain region, which are used to refine the brain nodes in the GNN for improved connectivity modeling in the next iteration. Through the iterative process, the global brain connectivity in the GNN and the local image features in the LFN are mutually enhanced, leading to accurate prognosis prediction. Extensive experiments on a public UCSF dataset of 493 diffuse glioma patients demonstrate that our framework outperforms the state-of-the-art methods. Further ablation studies reveal that the global brain connectivity is crucial and highly related to prognosis.

Keywords: prognosis prediction · global brain connectivity · local image features · compensatory mechanism

1 Introduction

Diffuse glioma is the most prevalent primary brain tumor, accounting for approximately 80% of malignant tumors in the central nervous system [13]. The prognosis of patients exhibits heterogeneity, ranging from months to over a decade [15].

In clinic, accurate prognosis prediction, which estimates survival risks or overall survival (OS) times of patients, provides critical information to support individualized treatment and has been extensively studied.

In the early stage, radiomics based prognosis prediction methods were intensively studied. The basic idea is to extract handcrafted features from images, including first order statistics, shape descriptors, and gray level co-occurrence matrix (GLCM) features, based on which traditional machine learning models, such as random forest and support vector machine (SVM) [11], are built to predict the corresponding survival risks or OS times of patients. In recent years, with the rapid development of deep learning (DL) networks, many DL based prognosis prediction methods have been proposed [20–22, 32]. Instead of handcrafted features, they leverage the powerful data-driving ability of DL networks to derive effective prognosis-related features from local image feature based methods images. Although both radiomics and DL based methods have achieved great success, most of them focus solely on local image features of tumor regions. It is known that the brain is an integrated and highly interconnected system, and tumors not only have impacts on local brain regions but also disrupt global brain connectivity, which is closely associated with prognosis and should be regarded as an important factor.

To address these issues, a new heterogeneous framework that integrates both global and local information for prognosis prediction of diffuse glioma is proposed in this paper. Specifically, our framework is composed of a DTI based GNN for exploring the global brain connectivity and a structural MR (sMR) based local feature network (LFN) for deriving features from local brain regions. Our framework works in an iterative manner, and in each iteration, the LFN leverages the global brain connectivity modeled by the GNN to derive local features of each brain region from sMR images. The resulting brain regional features are then used to refine the corresponding brain nodes in the GNN for improved global brain connectivity modeling in the next iteration. Therefore, through iteration, the global brain connectivity and local features of brain regions are mutually enhanced. Moreover, the compensatory mechanism (i.e., adaptive reorganization of brain region connections in response to tumors), which is highly associated with prognosis [5], is explicitly incorporated into the modeling of global brain connectivity. Based on the global brain connectivity and the local features of brain regions, accurate prediction of survival risks can be achieved.

The main contributions of our study are listed as follows:

- A new heterogeneous framework is proposed which integrates compensation-aware global brain connectivity with local brain region features in an iterative pipeline for the prognosis prediction of diffuse glioma.
- The global brain connectivity modeled by the DTI based GNN and the local brain region features extracted by the sMR based LFN are mutually refined across iterations, leading to accurate prognosis prediction.
- The compensatory mechanism of diffuse glioma, which reflects the adaptive reorganization of global brain connectivity and is an important prognosis-related factor, is explicitly incorporated into our framework.

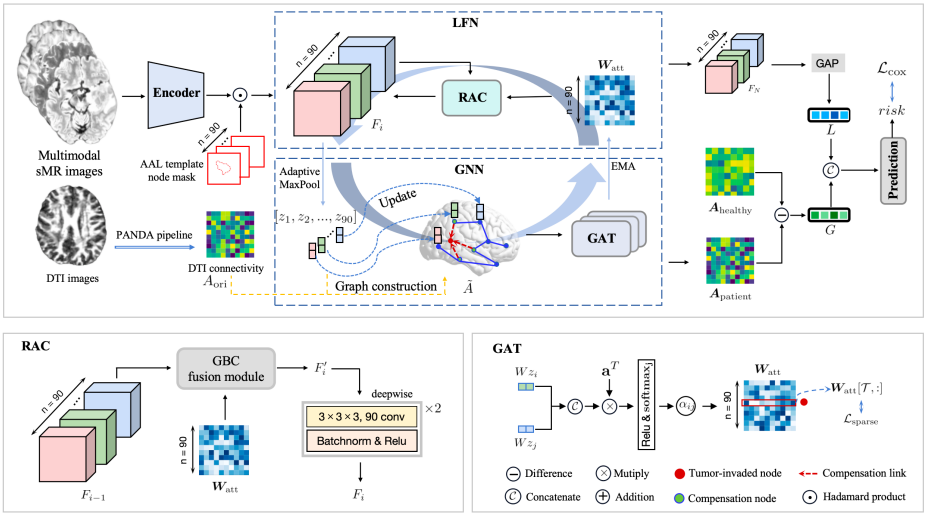

Fig. 1. Our framework is composed of a DTI based graph neural network (GNN) and a structural MR (sMR) based local feature network (LFN), which are operated in an iterative manner.

– Our framework outperforms 14 state-of-the-art methods on the public UCSF diffuse glioma dataset (493 patients). Ablation studies further confirm the effectiveness of global brain connectivity and compensatory mechanism.

2 Method

The architecture of our framework is shown in Fig. 1. It is composed of a DTI based GNN and a structural MR (sMR) based local feature network (LFN), which are coupled in an iterative manner. At each iteration, the LFN leverages the global brain connectivity modeled by the GNN to derive improved local features of each brain region from sMR images. These features are then fed into the corresponding nodes in the GNN for improved global brain connectivity modeling in the next iteration. The final global and local features are fused to predict patient survival risk, and we explicitly incorporate the compensatory mechanism into the GNN for comprehensive modeling of global brain connectivity. Details of each component of our framework are discussed in the following sections.

2.1 The DTI based GNN with brain compensation awareness

Graph construction. We build $\mathcal{G} = (\mathcal{V}, \mathcal{E})$ from DTI, where the nodes $\mathcal{V}$ are 90 brain regions defined by AAL-90 [24] template and edges come from white matter tracts using PANDA [3]. To reduce the influence of tumor mass effect on atlas registration, ANTs-based nonlinear registration with lesion masking [28]

is adopted. Thresholding with 0.2 is applied to the resulting white matter density matrix A_{ori} to obtain the graph edges represented by the binary adjacent matrix A. In clinic, it is known that compensation for tumor-invaded regions occurs mainly in peritumoral and contralateral regions [5, 14]. We partition $\mathcal{V}$ into tumor-invaded $\mathcal{T}$ (tumor voxel ratio $> 40\%$), peritumoral $\mathcal{P}$, contralateral $\mathcal{C}$, and others $\mathcal{R}$, and define the compensation-aware adjacency $\tilde{A}$ as

$$\tilde{A}_{ij} = \begin{cases} 1, & \text{if } A_{ij} = 1 \text{ and } i, j \notin \mathcal{T}, \\ 1, & \text{if } i \in \mathcal{T}, j \in \mathcal{P} \cup \mathcal{C} \text{ or } j \in \mathcal{T}, i \in \mathcal{P} \cup \mathcal{C}, \\ 0, & \text{otherwise.} \end{cases} \tag{1}$$

GAT backbone. We use graph attention network (GAT) [26] as the GNN backbone. The initial node features $Z = [z_1, \ldots, z_{90}] \in \mathbb{R}^{d \times 90}$ are derived from the corresponding brain region in the sMR based LFN (Sec. 2.2). Moreover, we concatenate the i-th row of A_{ori} (connectivity pattern) with z_i, yielding the final node feature $\hat{z}_i \in \mathbb{R}^{d+90}$. At each GAT layer, $\hat{z}_i$ is updated by

$$\hat{z}_i' = \|_{k=1}^{K} \text{ReLU}\left(\sum_{j \in \mathcal{N}_{\tilde{A}}(i)} \alpha_{ij}^{(k)} W^{(k)} \hat{z}_j \right), \tag{2}$$

where K is the number of attention heads, $\mathcal{N}_{\tilde{A}}(i) = \{j \mid \tilde{A}_{ij} = 1\}$ contains all neighbors of the i-th node, $W^{(k)}$ is the learnable k-th head's weight matrix, $\|$ denotes concatenation, and the attention coefficients $\alpha_{ij}^{(k)}$ are defined as

$$\alpha_{ij}^{(k)} = \frac{\exp\left(\text{LeakyReLU}\left(\mathbf{a}^{(k)\top}[W^{(k)}\hat{z}_i \| W^{(k)}\hat{z}_j]\right)\right)}{\sum_{l \in \mathcal{N}_{\tilde{A}}(i)} \exp\left(\text{LeakyReLU}\left(\mathbf{a}^{(k)\top}[W^{(k)}\hat{z}_i \| W^{(k)}\hat{z}_l]\right)\right)}, \tag{3}$$

where $\mathbf{a}^{(k)}$ is learnable attention vector. It is worth noting that in the last layer, multi-head outputs are averaged instead of concatenated. Motivated by the evidence that compensation relies on a limited set of regions [5], we add a new sparsity loss on the attention coefficients for nodes in $\mathcal{T}$ (tumor-invaded):

$$\mathcal{L}_{\text{sparse}} = \frac{1}{|\mathcal{T}|} \sum_{i \in \mathcal{T}} \left(- \sum_{j \in \mathcal{N}_{\tilde{A}}(i)} \alpha_{ij} \log \alpha_{ij} \right). \tag{4}$$

The GNN stacks three GAT layers for high-order aggregation. In the last layer, a global attention matrix is constructed:

$$W_{\text{att}} = \frac{1}{K} \sum_{k=1}^{K} \left[\alpha_1^{(k)\top}; \ldots; \alpha_{90}^{(k)\top} \right]^\top \in \mathbb{R}^{90 \times 90}, \tag{5}$$

where $\alpha_i^{(k)} = [\alpha_{i,1}^{(k)}, \ldots, \alpha_{i,90}^{(k)}] \in \mathbb{R}^{90}$. W_{att} encodes global brain connectivity and is used to guide local feature extraction in the LFN.

2.2 The sMR based LFN with guidance of global brain connectivity

Region-aware channels. The LFN extracts local features per brain region from multimodal sMR (T1, T1c, T2, FLAIR). Specifically, an image encoder in the LFN first yields $F \in \mathbb{R}^{H\times W\times D}$, which is further parcellated into 90 channel features F_0 using the AAL-90 template:

$$F_0 = [F \odot M_1, ..., F \odot M_{90}] \in \mathbb{R}^{H\times W\times D\times 90}, \tag{6}$$

where M_i is the binary mask of the i-th AAL-90 brain region.

RAC block. The LFN contains a region-aware convolutional (RAC) block (Fig. 1), which has a global brain connectivity guided (GBC) fusion module followed by a convolutional block. As aforementioned, our framework operates in an iterative manner. At the i-th iteration, the input of the RAC block is F_{i-1} (F_0 is from region parcellation above), and the GBC module fuses F_{i-1} by W_{att} from the GNN:

$$F_i' = D_{W_{\text{att}}}^{-1} W_{\text{att}} F_{i-1}^T[:, H, W, D], \tag{7}$$

where $D_{W_{\text{att}}}$ is the degree matrix of W_{att}. F_i' is fed to two $3\times 3\times 3$ depth-wise convolutional blocks (with BN+ReLU), yielding the output feature map F_i (i.e., the input for the next iteration).

After each iteration, AdaptiveMaxPool is applied to F_i to get $Z = [z_1, \ldots, z_{90}]$ which are used to update the GNN node features for the next iteration. It is worth noting that since no node features in GNN (i.e., no W_{att}) in the first iteration, $\tilde{A}$ is adopted instead of W_{att}.

2.3 Survival risk prediction with GNN and LFN

Based on empirical observations, the iteration can reach convergence (i.e., W_{att} and Z are stable) within six iterations. The prognosis is predicted according to the global brain connectivity W_{att} from GNN and the local image features F_6 from LFN after the 6-th iteration. Specifically, since alterations of brain connectivity between brain tumor patients and healthy individuals are prognosis-related [28]. An adjacent matrix of for healthy individuals $A_{\text{healthy}} \in \mathbb{R}^{90\times 90}$ is built by averaging DTI adjacency matrices of 387 healthy controls from Cam-CAN [23]. The patient adjacent matrix is built by

$$A_{\text{patient}} = (I + M_{\mathcal{T}} W_{\text{att}}) A_{\text{ori}}, \tag{8}$$

where I is the identity matrix and $M_{\mathcal{T}} \in \mathbb{R}^{90\times 90}$ is a row-wise mask defined as:

$$(M_{\mathcal{T}})_{ii} = \begin{cases} 1, & i \in \mathcal{T} \\ 0, & \text{otherwise} \end{cases}. \tag{9}$$

Therefore, the connections of the tumor-invaded brain regions in A_{patient} are defined by fusing the connections of the corresponding compensatory brain regions.

Then the brain connectivity alteration is defined as $G = \frac{1}{90}\sum_{i=1}^{90} |[A_{\text{patient}}]_i - [A_{\text{healthy}}]_i| \in \mathbb{R}^{90}$, where $[A_{\text{patient}}]_i$ and $[A_{\text{healthy}}]_i$ are the i-th row of the corresponding matrices. Based on the local brain features F_6 from the LFN, a global average pooling (GAP) is applied to get the local features $L \in \mathbb{R}^{90}$. The final features $x = [G\|L]$, encoding both global brain connectivity and local brain region features, are feed to the prediction head (MLP, 180→64→1) to predict the prognosis (survival risk) trained with the Cox loss:

$$\mathcal{L}_{\text{cox}} = -\sum_{i=1}^{N} \delta_i \left(\phi_\theta(I_i) - \log \sum_{j \in S(t_i)} e^{\phi_\theta(I_j)} \right), \tag{10}$$

where $\phi_\theta(I_i)$ is the predicted risk, $S(t_i)$ is the at-risk set at time t_i, and δ_i is the censoring indicator.

Our framework is unrolled six times for end-to-end training. The total loss is

$$\mathcal{L}_{\text{total}} = \mathcal{L}_{\text{cox}} + \lambda \mathcal{L}_{\text{sparse}}, \tag{11}$$

where λ is set to 0.5. Our framework is trained using Adam optimizer with learning rate of 1×10^{-4}, batch size of 16, and maximum of 100 training epochs.

3 Experiments

A public dataset of diffuse glioma UCSF [2] containing DTI and multimodal sMR (T1, T2, T1c, and FLAIR) images of 493 patients with histologically confirmed diffuse gliomas is adopted to evaluate our framework. To mitigate potential domain shift between UCSF and the healthy controls data (Cam-CAN), ComBat harmonization [19] is applied at preprocessing stage. Besides our framework, 14 state-of-the-art (SOTA) methods are included in our experiment, which can be divided into two groups: the local image feature based (LIF) group and the global brain connectivity based (GBC) group. Specifically, the LIF group contains the traditional radiomics based method Ra-MLP [1], the deep learning based method M^{2}Net [32], the deep survival model DeepSurv [10], the phenotype and genotype based method PG-OS [21], and the two Transformer based methods FACGL [30] and TMSS [18]. The GBC group contains the GCN [12], the GAT [26], the BNT [9], the dwHGCN [27], and the LG-GNN [31] , all of which rely solely on DTI data with node features defined by connectivity information. In addition, the R2SNs [7], the IDH-GNN [29], and the MaskGNN [16] in the GBC group are based on both DTI and sMR images, where graph node features are defined by the sMR images. All methods under evaluation are trained using the Cox loss, and five-fold cross validation is employed in the experiment. Four different metrics, including the concordance index (C-index) [6], the inverse probability of censoring weighted C-index (IPCW-CI) [25], the mean time-dependent area under the receiver operating characteristic curve (mAUC) [8], and the mean absolute error (MAE) [17], are used to quantify the prediction performance.

The evaluation results of all methods are shown in Table 1. Our framework achieves the best performance of all SOTA methods in terms of C-index, IPCW-CI, and mAUC. The MAE of our framework is also comparable to the best-performing method FACGL. It can be observed that methods in the LIF based group show better performance than those in the GBC based group, indicating that local image features may encode richer prognosis-related information than global brain connectivity. In the GBC based group, methods relying solely on DTI images exhibit relatively low predictive performance, such as GCN, GAT, BNT, dwHGCN, and LG-GNN. In contrast, other GBC based methods incorporating sMR images, including DC-R2SNs, IDH-GNN, and MaskGNN, achieve superior performance over the methods based on DTI images only.

Table 1. Evaluation results of survival risk prediction.

	Method	C-index ↑	IPCW-CI ↑	mAUC ↑	MAE ↓
LIF based group	Ra-MLP [1]	0.650 ± 0.051	0.635 ± 0.057	0.687 ± 0.073	24.4 ± 4.81
	M^2Net [32]	0.709 ± 0.010	0.686 ± 0.010	0.765 ± 0.011	24.9 ± 3.45
	DeepSurv [10]	0.647 ± 0.041	0.634 ± 0.044	0.680 ± 0.062	25.8 ± 3.90
	PG-OS [21]	0.664 ± 0.035	0.647 ± 0.033	0.702 ± 0.051	25.8 ± 3.82
	FACGL [30]	0.696 ± 0.028	0.684 ± 0.019	0.744 ± 0.049	**22.2 ± 3.40**
	TMSS [18]	0.703 ± 0.031	0.686 ± 0.028	0.756 ± 0.050	24.6 ± 3.61
GBC based group	GCN [12]	0.654 ± 0.033	0.639 ± 0.031	0.691 ± 0.052	27.7 ± 3.51
	GAT [26]	0.659 ± 0.045	0.632 ± 0.048	0.685 ± 0.070	26.5 ± 4.02
	BNT [9]	0.669 ± 0.022	0.651 ± 0.034	0.698 ± 0.044	26.0 ± 5.01
	dwHGCN [27]	0.666 ± 0.041	0.656 ± 0.049	0.707 ± 0.065	26.7 ± 5.23
	LG-GNN [31]	0.661 ± 0.032	0.657 ± 0.044	0.700 ± 0.051	30.4 ± 5.62
	DC-R2SNs [7]	0.693 ± 0.017	0.675 ± 0.022	0.742 ± 0.042	24.2 ± 3.68
	IDH-GNN [29]	0.692 ± 0.052	0.666 ± 0.053	0.732 ± 0.068	23.5 ± 5.02
	MaskGNN [16]	0.684 ± 0.034	0.662 ± 0.030	0.728 ± 0.052	23.0 ± 3.15
	Ours	**0.717 ± 0.010**	**0.691 ± 0.011**	**0.776 ± 0.013**	22.3 ± 3.68

Ablation Study. Our framework without the GNN, without the LFN, and without the iteration pipeline are evaluated. It is worth noting that for our framework without the LFN, features for each graph node is defined by the adjacent matrix $\tilde{A}$. Moreover, our framework without the brain compensation awareness is also tested, where the adjacent matrix is A instead of $\tilde{A}$ and no sparse constraint $\mathcal{L}_{\text{sparse}}$ is applied. The ablation results are included in Table 2. It can be observed that both components are essential to our framework.

Sensitivity Analysis. Across tumor-voxel thresholds of 30%–60%, the corresponding C-index varies from 0.711 to 0.717, indicating stable performance, with the 40% threshold achieving the highest C-index of 0.717. For the number of unrolling iterations, both the attention matrix and brain-region features converge within six iterations, and additional iterations do not improve performance but increased computational cost.

Table 2. Evaluation results of ablation study.

Method	C-index ↑	IPCW-CI ↑	mAUC ↑	MAE ↓
w/o GC*	0.688 ± 0.026	0.662 ± 0.025	0.697 ± 0.019	25.5 ± 4.41
w/o LF*	0.676 ± 0.056	0.650 ± 0.041	0.677 ± 0.033	27.1 ± 5.66
w/o Iteration	0.701 ± 0.016	0.666 ± 0.042	0.758 ± 0.031	23.8 ± 3.88
w/o Compensation	0.709 ± 0.016	0.683 ± 0.049	0.767 ± 0.036	23.5 ± 3.37
Ours	**0.717 ± 0.010**	**0.691 ± 0.011**	**0.776 ± 0.013**	**22.3 ± 3.68**

*GC: global brain connectivity; LF: local image features.

Case Study. Our framework contains an iterative pipeline, where the global brain connectivity in the GNN and the local image features in the LFN are mutually improved until convergence, i.e., the global attention matrix W_{att} is stable. Fig. 2 visualizes W_{att} after each iteration, where W_{att} changes drastically in the early iterations and gradually converges as the iteration proceeds. The high values in W_{att} indicate strong correlation between two brain regions.

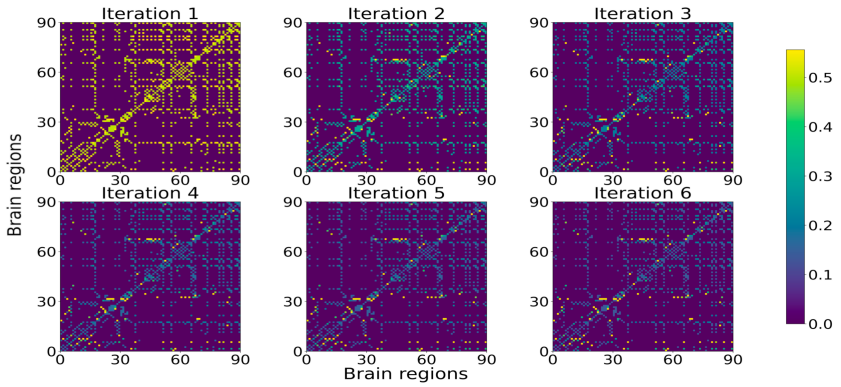

Fig. 2. Visualization of W_{att} after iterations 1-6 in our framework.

Fig. 3 shows two examples of the compensation brain regions. Specifically, for the tumor-invaded brain regions of each patient (marked in blue), the effective compensation regions are determined in the GNN as defined in (5). It can be observed that in the low-grade tumor, compensation is in peritumoral regions, whereas in the high-grade tumor, it shifts to contralateral regions, consistent with clinical evidence [4].

4 Conclusion

We proposed a heterogeneous framework for diffuse glioma prognosis prediction that jointly models global brain connectivity and local image features in an iterative optimization pipeline. Compensation mechanism is incorporated to capture adaptive reorganization of brain connectivity caused by tumor disruption. Exper-

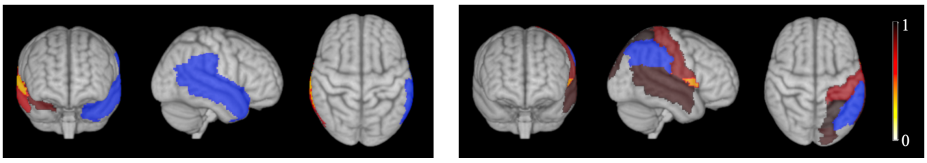

Fig. 3. Compensation region distribution for low-grade (left) and high-grade (right) glioma patients. Tumor-invaded brain regions are marked in blue, and compensatory regions represented by different colors indicate corresponding weights.

iments on the UCSF dataset show superior performance over 14 state-of-the-art methods, with ablation studies confirming the contribution of each component.

Acknowledgments. This work is supported by the National Natural Science Foundation of China (Grant No. 62572023) and the Key Research and Development Program of China (Grant Nos. 2023YFC2411001 and 2023YFC2411002).

Disclosure of Interests. The authors have no competing interests.

References

1. Baid, U., Rane, S.U., Talbar, S., Gupta, S., Thakur, M.H., Moiyadi, A., Mahajan, A.: Overall survival prediction in glioblastoma with radiomic features using machine learning. Frontiers in Computational Neuroscience **14**, 61 (2020)
2. Calabrese, E., Villanueva-Meyer, J.E., Rudie, J.D., Rauschecker, A.M., Baid, U., Bakas, S., Cha, S., Mongan, J.T., Hess, C.P.: The University of California San Francisco preoperative diffuse glioma MRI dataset. Radiology: Artificial Intelligence **4**(6), e220058 (2022)
3. Cui, Z., Zhong, S., Xu, P., He, Y., Gong, G.: PANDA: a pipeline toolbox for analyzing brain diffusion images. Frontiers in Human Neuroscience **7**, 42 (2013)
4. Desmurget, M., Bonnetblanc, F., Duffau, H.: Contrasting acute and slow-growing lesions: a new door to brain plasticity. Brain **130**(4), 898–914 (2007)
5. Duffau, H.: The huge plastic potential of adult brain and the role of connectomics: new insights provided by serial mappings in glioma surgery. Cortex **58**, 325–337 (2014)
6. Harrell Jr, F.E., Lee, K.L., Mark, D.B.: Multivariable prognostic models: issues in developing models, evaluating assumptions and adequacy, and measuring and reducing errors. Statistics in Medicine **15**(4), 361–387 (1996)
7. Hu, X., Xiao, L., Wang, Y.P.: A graph neural network based fusion of MRI-derived brain network and clinical data for glioblastoma survival prediction. In: ICASSP. pp. 1571–1575. IEEE (2024)
8. Hung, H., Chiang, C.T.: Estimation methods for time-dependent AUC models with survival data. Canadian Journal of Statistics **38**(1), 8–26 (2010)
9. Kan, X., Dai, W., Cui, H., Zhang, Z., Guo, Y., Yang, C.: Brain network transformer. In: NeurIPS. vol. 35, pp. 25586–25599 (2022)
10. Katzman, J.L., Shaham, U., Cloninger, A., Bates, J., Jiang, T., Kluger, Y.: DeepSurv: personalized treatment recommender system using a Cox proportional hazards deep neural network. BMC Medical Research Methodology **18**(1), 24 (2018)

11. Kickingereder, P., Burth, S., Wick, A., Götz, M., Eidel, O., Schlemmer, H.P., Maier-Hein, K.H., Wick, W., Bendszus, M., Radbruch, A., et al.: Radiomic profiling of glioblastoma: identifying an imaging predictor of patient survival with improved performance over established clinical and radiologic risk models. Radiology **280**(3), 880–889 (2016)
12. Kipf, T.N., Welling, M.: Semi-supervised classification with graph convolutional networks. In: ICLR (2017)
13. Louis, D.N., Perry, A., Wesseling, P., Brat, D.J., Cree, I.A., Figarella-Branger, D., Hawkins, C., Ng, H.K., Pfister, S.M., Reifenberger, G., Soffietti, R., von Deimling, A., Wiestler, O.D., Ellison, D.W.: The 2021 WHO classification of tumors of the central nervous system: a summary. Neuro-Oncology **23**(8), 1231–1251 (2021)
14. Lv, K., Cao, X., Wang, R., Du, P., Fu, J., Geng, D., Zhang, J.: Neuroplasticity of glioma patients: brain structure and topological network. Frontiers in Neurology **13**, 871613 (2022)
15. Pellerino, A., Caccese, M., Padovan, M., Cerretti, G., Lombardi, G.: Epidemiology, risk factors, and prognostic factors of gliomas. Clinical and Translational Imaging **10**(5), 467–475 (2022)
16. Qu, G., Zhou, Z., Calhoun, V.D., Zhang, A., Wang, Y.P.: Integrated brain connectivity analysis with fMRI, DTI, and sMRI powered by interpretable graph neural networks. Medical Image Analysis **103**, 103570 (2025)
17. Reid, N.: Estimating the median survival time. Biometrika **68**(3), 601–608 (1981)
18. Saeed, N., Sobirov, I., Al Majzoub, R., Yaqub, M.: TMSS: An end-to-end transformer-based multimodal network for segmentation and survival prediction. In: MICCAI. pp. 319–329. Springer (2022)
19. Solanes, A., Gosling, C.J., Fortea, L., Ortuño, M., Lopez-Soley, E., Llufriu, S., Madero, S., Martinez-Heras, E., Pomarol-Clotet, E., Solana, E., et al.: Removing the effects of the site in brain imaging machine-learning – Measurement and extendable benchmark. NeuroImage **265**, 119800 (2023)
20. Tang, Z., Li, J., Cheng, J., Li, Z.C., Zhang, Z., Yan, J.: Pre-operative overall survival prediction of diffuse glioma enhanced by longitudinal data. IEEE Journal of Biomedical and Health Informatics **29**(7), 5158–5167 (2025)
21. Tang, Z., Xu, Y., Jin, L., Aibaidula, A., Lu, J., Jiao, Z., Wu, J., Zhang, H., Shen, D.: Deep learning of imaging phenotype and genotype for predicting overall survival time of glioblastoma patients. IEEE Transactions on Medical Imaging **39**(6), 2100–2109 (2020)
22. Tang, Z., Zhang, Z., Liu, H., Nie, D., Yan, J.: Pre-operative survival prediction of diffuse glioma patients with joint tumor subtyping. In: International Conference on Medical Image Computing and Computer-Assisted Intervention. pp. 786–795. Springer (2023)
23. Taylor, J.R., Williams, N., Cusack, R., Auer, T., Shafto, M.A., Dixon, M., Tyler, L.K., Henson, R.N., et al.: The Cambridge Centre for Ageing and Neuroscience (Cam-CAN) data repository: Structural and functional MRI, MEG, and cognitive data from a cross-sectional adult lifespan sample. NeuroImage **144**, 262–269 (2017)
24. Tzourio-Mazoyer, N., Landeau, B., Papathanassiou, D., Crivello, F., Etard, O., Delcroix, N., Mazoyer, B., Joliot, M.: Automated anatomical labeling of activations in SPM using a macroscopic anatomical parcellation of the MNI MRI single-subject brain. NeuroImage **15**(1), 273–289 (2002)
25. Uno, H., Cai, T., Pencina, M.J., D'Agostino, R.B., Wei, L.J.: On the c-statistics for evaluating overall adequacy of risk prediction procedures with censored survival data. Statistics in Medicine **30**(10), 1105–1117 (2011)

26. Veličković, P., Cucurull, G., Casanova, A., Romero, A., Liò, P., Bengio, Y.: Graph attention networks. In: ICLR (2018)
27. Wang, J., Li, H., Qu, G., Cecil, K.M., Dillman, J.R., Parikh, N.A., He, L.: Dynamic weighted hypergraph convolutional network for brain functional connectome analysis. Medical Image Analysis **87**, 102828 (2023)
28. Wei, Y., Li, C., Cui, Z., Mayrand, R.C., Zou, J., Wong, A.L.K.C., Sinha, R., Matys, T., Schönlieb, C.B., Price, S.J.: Structural connectome quantifies tumour invasion and predicts survival in glioblastoma patients. Brain **146**(4), 1714–1727 (2023)
29. Wei, Y., Li, Y., Chen, X., Schönlieb, C.B., Li, C., Price, S.J.: Predicting isocitrate dehydrogenase mutation status in glioma using structural brain networks and graph neural networks. In: International MICCAI Brainlesion Workshop. pp. 140–150. Springer (2021)
30. Yue, H., Liu, J., Kuang, H., Cheng, J., Li, J., Wang, J.: A fully automated CT-guided learning for survival prediction of esophageal cancer. In: 2023 IEEE International Conference on Bioinformatics and Biomedicine (BIBM). pp. 1670–1675. IEEE (2023)
31. Zhang, H., Song, R., Wang, L., Zhang, L., Wang, D., Wang, C., Zhang, W.: Classification of brain disorders in rs-fMRI via local-to-global graph neural networks. IEEE Transactions on Medical Imaging **42**(2), 444–455 (2023)
32. Zhou, T., Fu, H., Zhang, Y., Zhang, C., Lu, X., Shen, J., Shao, L.: M2Net: Multimodal multi-channel network for overall survival time prediction of brain tumor patients. In: International Conference on Medical Image Computing and Computer-Assisted Intervention. pp. 221–231. Springer (2020)